JOURNAL OF Applied Polymer SCIENCE

Effect of Phase Separation on Overall Isothermal Crystallization Kinetics of PP/EPR In-Reactor Alloys

Yi-Min Liu, Jun-Ting Xu, Zhi-Sheng Fu, Zhi-Qiang Fan

MOE Key Laboratory of Macromolecular Synthesis and Functionalization, Department of Polymer Science & Engineering, Zhejiang University, Hangzhou 310027, China

Correspondence to: J.-T. Xu (E-mail: xujt@zju.edu.cn)

ABSTRACT: In the present work, the effect of phase separation on overall isothermal crystallization kinetics of two polypropylene/ethylene-propylene random copolymer (PP/EPR) in-reactor alloys was investigated. It is found that at lower crystallization temperatures (T_c), the overall crystallization rate decreases with increasing phase separation temperature (T_s). This is attributed to the lower linear spherulitic growth rate incurred by the lower PP content in the PP-rich phase at higher T_ss. In contrast, at higher T_cs, quenching from a higher T_s to T_c promotes nucleation as a result of more dramatic concentration fluctuation, leading to a faster overall crystallization rate. The overall crystallization rate of the PP/EPR in-reactor alloy prepared by multi-stage sequential polymerization process (MSSP) is retarded by increasing phase separation time (t_s). However, prolonging phase separation time has little effect on the crystallization rate of the sample prepared by two-stage polymerization process (TSP). This result can be attributed to the different phase separation rates of these two samples. The SAXS result confirms that at higher T_c, phase separation in the melt before crystallization can retard crystallization, when compared with the directly quenched samples. It is also found that the phase-separated PP/EPR in-reactor alloys exhibit a larger long period because of more amorphous phases included between the lamellar crystals.

KEYWORDS: phase separation; isothermal crystallization; polypropylene; in-reactor alloy

Received 5 January 2012; accepted 13 March 2012; published online 00 Month 2012
DOI: 10.1002/app.37689

INTRODUCTION

Since the discovery of Catalloy process by Himont company, polypropylene (PP) in-reactor alloy has attracted many researchers because of its good balance in tensile strength and impact strength.[1,2] To further optimize the properties of PP in-reactor alloys, lots of studies have been devoted to the polymerization process, chain structure, crystallization behavior, and phase morphology of PP in-reactor alloys.[3–28] A two-stage polymerization process (TSP) is commonly used to produce polypropylene/ethylene-propylene random copolymer (PP/EPR) in-reactor alloys: propylene homopolymerization followed by ethylene-propylene copolymerization.[29–32] Recently, multi-zone circular reactor (MZCR) process and multi-stage sequential polymerization (MSSP) process were also developed for preparation of PP/EPR in-reactor alloys.[33–38]

Because of the nature of plural active sites in heterogeneous Ziegler-Natta catalyst and the TSP, the obtained PP/EPR in-reactor alloys are usually a mixture. The components in PP/EPR in-reactor alloys include PP homopolymer, EPR, ethylene-propylene multi-block copolymer, and sometimes polyethylene.[39–44]

In a multi-component system containing a crystalline component, the miscibility of the components in the melt has a vital effect on the crystallization behavior, and thus on morphology and final properties of the materials.[45–51] As a result, studying the effect of phase separation on crystallization is of great importance for multi-component systems containing a crystalline component. Han and co-workers observed that the nucleation energy barrier in crystallization could be overcome by the concentration fluctuation growth of liquid-liquid phase separation (LLPS) and proposed a "fluctuation-assisted nucleation" mechanism for the crystallization process in binary polyolefin blend systems.[52–55] Similar phenomenon was observed isotactic PP/poly(ethylene-*co*-octene) (iPP/PEOc) in-reactor alloys.[56–58] So far, although there are some studies on crystallization kinetics of PP/EPR in-reactor alloys,[59–61] the effect of phase separation is seldom considered in this type of in-reactor alloy. In our

Table I. Polymerization Conditions and Mechanical Properties of PP/EPR In-Reactor Alloys

	Retention time in each polymerization cycle (min)				
Sample	Propylene homopolymerization	Ethylene-propylene copolymerization	Switch number (times)	Impact strength (kJ/m^2)	Flexural modulus (MPa)
Sample 1	7.5	2.5	8	13.6	915.7
Sample 2	60	20	1	3.9	770.7

previous work, we reported the effect of phase separation in the melt on the linear spherulitic growth rate (G) of a PP/EPR in-reactor alloy prepared by MSSP process.[62] We found that higher phase separation temperature (T_s) led to a smaller G at lower crystallization temperatures (T_c), but phase separation had no significant effect on G at higher T_cs. This result was interpreted based on the phase diagram. In the present work, we will discuss the effect of phase separation on the overall crystallization rate of PP/EPR in-reactor alloys. For the overall crystallization rate, apart from the linear spherulitic growth rate of the PP-rich phase, the nucleation process and crystallization of the EPR-rich phase should also be considered. As a result, the effect of phase separation on the overall crystallization of PP/EPR in-reactor alloys would be more complicated.

In this work, two different thermal treatments, i.e., phase separation in the melt and quenching from homogeneous melt, were applied to the PP/EPR in-reactor alloys before crystallization, respectively. The isothermal crystallization behavior of PP/EPR in-reactor alloys was studied using differential scanning calorimetry (DSC) and the data were analyzed with Avrami theory. The nucleation process was investigated with polarized optical microscopy (POM). Time-resolved small angle X-ray scattering (SAXS) experiments were conducted as well. The effects of phase separation temperature (T_s) and phase separation time (t_s) on the isothermal crystallization behavior of PP/EPR in-reactor alloys were discussed based on both nucleation and linear spherulitic growth rate. This study may help us understand the influence of phase separation on crystallization behavior of PP/EPR in-reactor alloys and will give us a better comprehension for the relationships between the structure, morphology, and properties of the PP/EPR in-reactor alloys.

EXPERIMENTAL

Preparation of PP/EPR In-Reactor Alloys

Details for preparation of PP/EPR in-reactor alloys were described elsewhere.[38] An MSSP was conducted using a high yield spherical Ziegler-Natta catalyst, $TiCl_4/MgCl_2$·ID (where ID is an internal donor), kindly donated by BRICI, SINOPEC (Beijing, China). In the first stage, propylene homopolymerization was performed for 60 min after the prepolymerization conducted in a well-stirred glass reactor. Next was a circular reaction mode including ethylene-propylene copolymerization, in which an ethylene-propylene mixture of a constant composition (propylene/ethylene = 1.5) was continuously supplied to the autoclave under constant pressure (0.4 MPa) and propylene homopolymerization under constant pressure (0.6 MPa). That is to say, after ethylene-propylene copolymerization for a designed time, the polymerization was switched to propylene homopolymerization and subsequently ethylene-propylene copolymerization at the same conditions as above. The circular

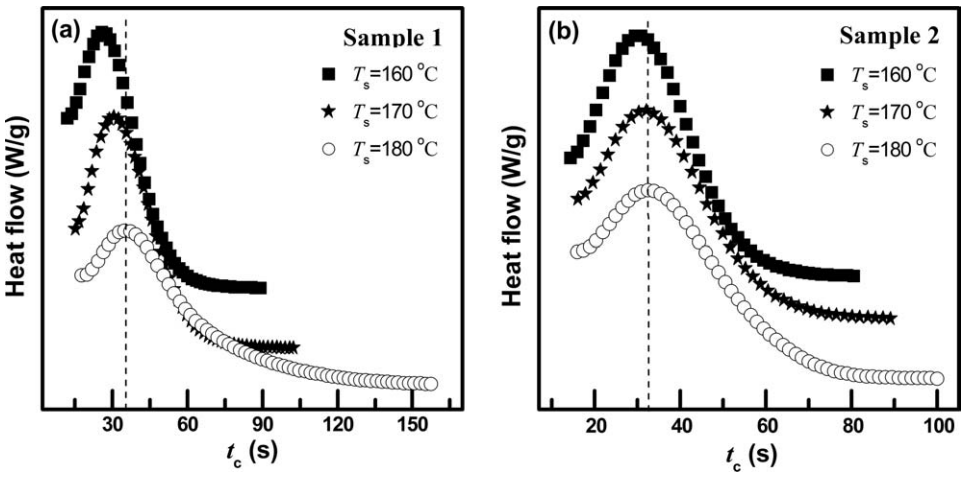

Figure 1. DSC traces of PP/EPR in-reactor alloys isothermally crystallized at 113°C after phase separation at various temperatures for 1 h. (a) Sample 1 and (b) Sample 2.

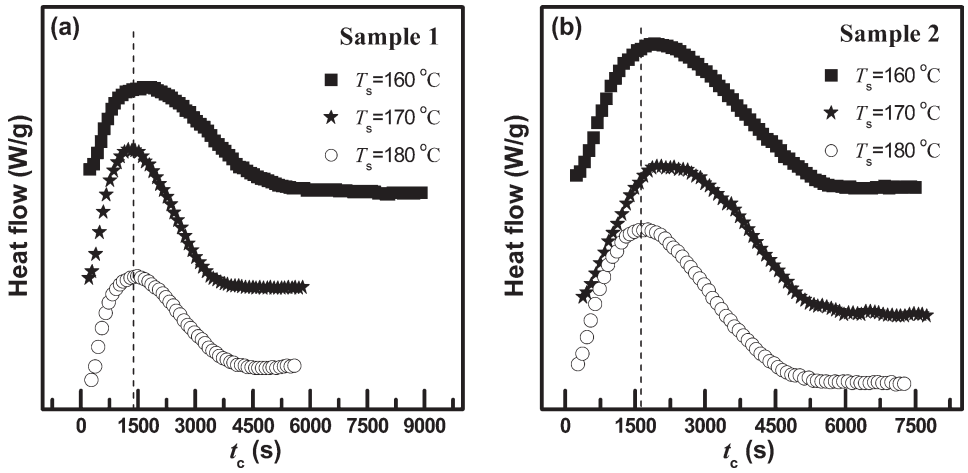

Figure 2. DSC traces of PP/EPR in-reactor alloys isothermally crystallized at 133°C after phase separation at various temperatures for 1 h. (a) Sample 1 and (b) Sample 2.

reaction mode was performed for 80 min at 60°C. Sample 1 was synthesized by ethylene-propylene copolymerization for 2.5 min and then propylene homopolymerization for 7.5 min in a circle and its switch times was 8. Sample 2 was prepared by a TSP process, in which the times for ethylene-propylene copolymerization and propylene homopolymerization are 20 min and 60 min, respectively. The polymerization parameters and mechanical properties of these two samples are given in Table I.[63]

DSC

Isothermal crystallization kinetics of the PP/EPR in-reactor alloys was performed on a TA Q-200 calorimeter. About 3–5 mg of the samples was sealed with aluminum pans for each experiment. There were two different thermal treatments that were applied to the samples before isothermal crystallization. In the first thermal treatment (named direct quench process), the samples were first melted at 230°C for 5 min to eliminate thermal history then cooled directly from 230°C to the pre-set crystallization temperature (T_c) at a rate of 40°C/min to complete isothermal crystallization. In the second thermal treatment (named phase separation process), the samples were first melted at 230°C for 5 min to eliminate thermal history, then quenched to a phase separation temperature (T_s) and held for a period of time (t_s) to facilitate phase separation and then cooled to the pre-set crystallization temperature (T_c) at a rate of 40°C/min to complete isothermal crystallization. The change of heat flow with time was recorded on crystallization. After isothermal crystallization was completed, the samples were heated to 230°C immediately from the crystallization temperature at a rate of 10°C/min. Overall crystallization rates under isothermal conditions are generally analyzed with the so-called Avrami equation,[64] as given in the following equation:

$$1 - X(t) = \frac{\Delta H^c_{t=\infty} - \Delta H^c_t}{\Delta H^c_{t=\infty} - \Delta H^c_{t=0}} = \exp(-kt^n) \quad (1)$$

where $X(t)$ is the relative crystallinity at time t, and $\Delta H^c_{t=\infty}$, $\Delta H^c_{t=0}$, and ΔH^c_t are the crystallization enthalpies on complete crystallization ($t = \infty$), at $t = 0$, and after time t, respectively. Therefore, we have:

$$\log\{-\ln[1 - X(t)]\} = \log k + n \log t \quad (2)$$

The crystallization rate constant k and Avrami exponent n can be determined from the intercept and slope in the plot of log $\{-\ln[1 - X(t)]\}$ versus log t, respectively. The crystallization half-time $t_{1/2}$ is related to the crystallization rate constant and Avrami exponent by the following equation:

$$\log(t_{1/2}) = [\log(\ln 2) - \log k]/n \quad (3)$$

Polarized Optical Microscopy

A polarized optical microscope (Olympus BX-51) equipped with a hot-stage and a digital camera was used to monitor the morphological evolution of PP/EPR in-reactor alloys during crystallization under different thermal treatment conditions. The same two different thermal treatments as that in DSC were applied to the samples before isothermal crystallization. In the directly quench process, the samples were first melted at 230°C for 5 min to eliminate thermal history, then cooled directly to the pre-set crystallization temperature (T_c) at a rate of 40°C/min for isothermal crystallization. In the phase separation process, the samples were first melted at 230°C for 5 min to eliminate thermal history, then quenched to a phase separation temperature (T_s) and held for a period of time (t_s) to facilitate phase separation, and then cooled to the pre-set crystallization temperature (T_c) at a rate of 40°C/min for isothermal crystallization.

SAXS and Data Analysis

SAXS experiments were performed at BL16B1 beamline in Shanghai Synchrotron Radiation Facility (SSRF) in China. The wavelength was 1.24 Å and sample-to-detector distance was set as 5100 mm. Two-dimensional (2D) SAXS patterns were recorded by time-resolved mode during isothermal crystallization process. The average exposure time was 300 s for each scan. The bull tendon was used as standard

Applied Polymer SCIENCE

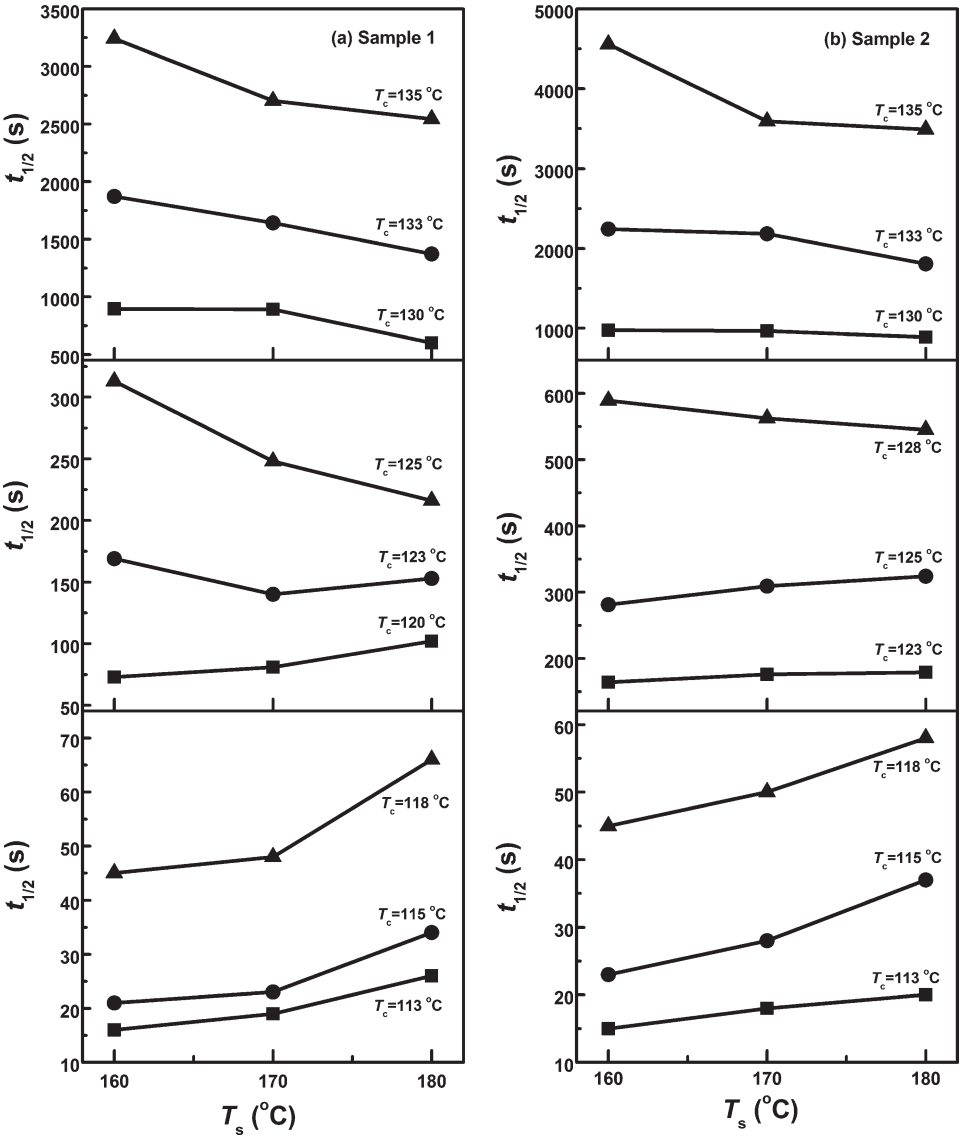

Figure 3. Variations of crystallization half-time ($t_{1/2}$) with phase separation temperature (T_s) at various crystallization temperatures. (a) Sample 1 and (b) Sample 2.

material for calibrating the scattering vector. The 2D SAXS patterns were converted into one-dimensional (1D) SAXS profiles using Fit2D software. Two different thermal treatments were applied to the samples at a Linkam hot-stage before SAXS experiments. In the first thermal treatment, the samples were firstly eliminated any thermal history at 230°C for 5 min, then cooled to 140°C at a rate of 40°C/min to conduct isothermal crystallization. In the second thermal treatment, the samples were quenched to 180°C and held for 1 h to facilitate phase separation after elimination of thermal history, and then cooled to 140°C for isothermal crystallization. SAXS experiments started when the temperature reached the pre-set T_c.

All the SAXS data were corrected by subtracting the background and were plotted in a Lorentz-corrected form, Iq^2 versus q, where q is the scattering vector given by:

$$q = 4\pi \sin \theta/\lambda \tag{4}$$

where λ is the wavelength and 2θ is the scattering angle.

The scattering invariant, Q is defined as:

$$Q = \int_0^\infty I(q)q^2 dq \tag{5}$$

The scattering invariant is proportional to the square of the electron density difference between the crystalline and amorphous phases, $(\rho_c\text{-}\rho_a)^2$, and the volume fraction of the crystalline phase $(X_s\phi_c)$, where X_s is the volume fraction of spherulites and ϕ_c is the volume crystallinity within the lamellar stacks [eq. (6)].[65]

$$Q \propto X_s\phi_c(1-\phi_c)(\rho_c-\rho_a)^2 \tag{6}$$

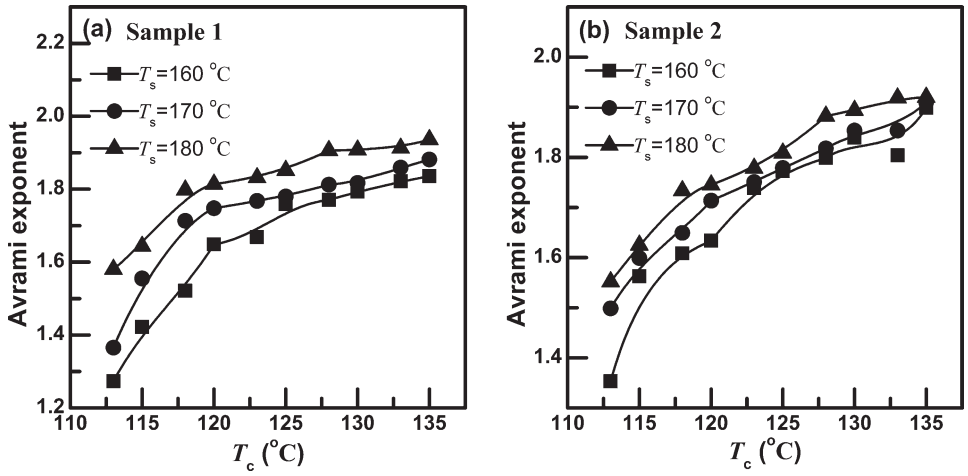

Figure 4. Plots of Avrami exponents versus crystallization temperature for PP/EPR in-reactor alloys after phase separation at different temperatures for 1 h. (a) Sample 1 and (b) Sample 2.

However, because the SAXS experiments were performed in a limited q range, we just calculated the scattering invariant in the experimental range (from $q = 0.18$ to $q = 0.75$) to yield Q':

$$Q' = \int_{0.18}^{0.75} I(q)q^2 dq \tag{7}$$

RESULTS AND DISCUSSION

Effect of Phase Separation Temperature

As revealed by our previous work, the phase diagram of PP/EPR in-reactor alloys is upper critical solubility temperature (UCST) type, the phase transition temperatures are about 182°C for Sample 1 and 205°C for Sample 2, respectively,[63] therefore we choose 160°C, 170°C, and 180°C as the phase separation temperatures in this work. At each experimental run, the PP/EPR in-reactor alloy was first held at 230°C for 5 min. At this temperature, not only the thermal history is eliminated but also the alloy becomes miscible and homogeneous.

Figures 1 and 2 show the heat flow traces of two samples crystallizing at two representative crystallization temperatures: one lower T_c (113°C) and one higher T_c (133°C). At T_c = 113°C, the time to reach the peak of heat flow (t_p) increases with increasing T_s. This phenomenon is especially evident for the Sample 1. The increase of t_p means that the decrease of crystallization rate. In contrast, the change of t_p with T_s is just opposite at T_c = 133°C. The data in Figure 2 shows that t_p decreases with T_s, indicating that the crystallization rate becomes faster after phase separation at higher T_s. Comparing the results in Figures 1 and 2, one can see that the effect of phase separation on the overall crystallization rate of PP/EPR in-reactor alloys strongly depends on crystallization temperature. To further verify this finding, the crystallization half-time ($t_{1/2}$) was also calculated based on eq. (3). The variations of $t_{1/2}$ with phase separation temperature (T_s) at various crystallization temperatures were presented in Figure 3. The crystallization half-time is defined as the time required to reach half of the final crystallinity. Usually, $t_{1/2}$ is a measurement of the overall crystallization

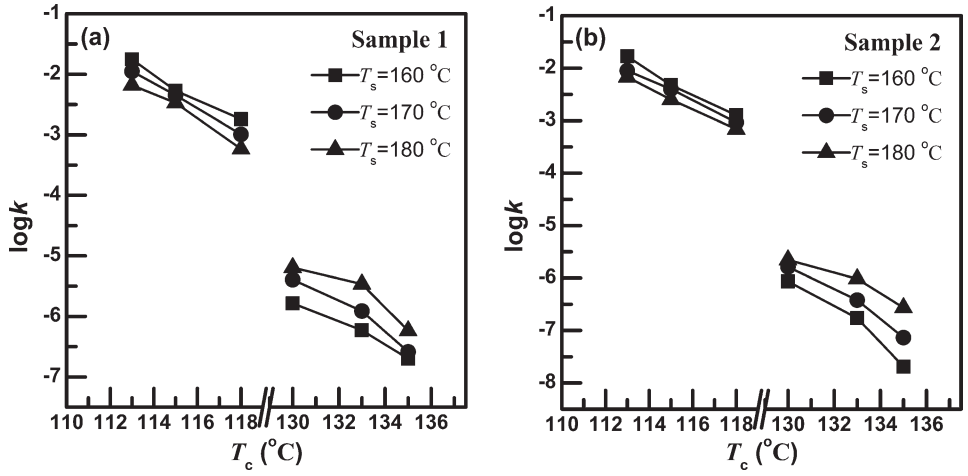

Figure 5. Plots of log k versus crystallization temperature for PP/EPR in-reactor alloys after phase separation at different temperatures for 1 h. (a) Sample 1 and (b) Sample 2.

rate. The larger the value of $t_{1/2}$, the slower the overall crystallization rate. As shown in Figure 3(a), when T_c is below 123°C, $t_{1/2}$ of Sample 1 increases with the T_s. On the contrary, when Sample 1 crystallized at higher T_cs ($T_c \geq 123$°C), $t_{1/2}$ decreases with increasing the T_s. Similar phenomenon was observed for Sample 2 prepared by TSP process [Figure 3(b)]. The variation of $t_{1/2}$ with T_s is in accordance with that of t_p shown in Figures 1 and 2. As a result, both the results of t_p and $t_{1/2}$ reveal that the effect of phase separation temperature on the overall crystallization rate of PP/EPR in-reactor alloys is different at lower and higher crystallization temperatures.

At lower crystallization temperatures, the degree of supercooling for crystallization is higher, resulting in a faster nucleation rate after both thermal treatments. Therefore, the linear spherulitic growth rate is the decisive factor for the differences in the overall crystallization rate under various phase separation conditions. This can be seen from the effects of phase separation temperature on the Avrami exponent (n) and crystallization rate constant (k), as shown in Figures 4 and 5. It is found that in the crystallization temperature range investigated in the present work, a higher T_s always leads to a larger Avrami exponent. This result holds true for both PP/EPR in-reactor alloys. However, for the crystallization rate constant k, the situation is different. The effect of T_s on k is strongly dependent on crystallization temperature. At lower T_cs, the value of k decreases as T_s increases, whereas it increases with T_s at higher T_cs. Based on eq. (3), the crystallization half-time $t_{1/2}$ is inversely proportional to both k and n. As a result, the decrease of k with increasing T_s is the predominant factor responsible for the increase of $t_{1/2}$ with T_s at lower T_cs. Because the value of k is proportional to linear growth rate and growth dimension of polymer crystals, the decrease of k with T_s at lower T_cs implies that the linear spherulitic growth rate also decreases with T_s. This is exactly what we observed in our previous work and can be explained in terms of the phase diagram (Figure 6).[62] Because of the faster crystallization rate at lower crystallization temperatures, the secondary phase separation, which is the phase separation occurring at T_c following the phase separation at T_s, is avoided. In such a situation, the PP-rich phase starts crystallization from the composition at the phase separation temperature, instead of the composition at the crystallization temperature. As shown in Figure 6, the PP content in the PP-rich phase is c_1 at the higher phase separation temperature (T_s^1) and c_2 at the lower phase separation temperature (T_s^2), respectively. A higher phase separation temperature leads to a lower PP content in the PP-rich phase ($c_2 > c_1$). When the melts were cooled to T_c, the starting compositions for crystallization of the PP-rich phase are accordingly c_1 and c_2. The higher PP content in the PP-rich phase (c_2) at T_s^2 leads to a higher linear spherulitic growth rate. Finally, the larger linear spherulitic growth rate results in a faster overall crystallization rate at a lower T_s.

Noting that, in Figure 4, the Avrami exponents obtained are in the range of 1.0–2.0. These values are far below the Avrami exponent for the spherulitic growth of polymer crystals, which was observed in our previous work.[63] The Avrami exponent for the spherulitic growth should be around 3.0 for a heterogeneous nucleation process and 4.0 for a homogeneous nucleation process. The Avrami exponents and crystallization rate constants obtained by DSC are indeed apparent values, which are the averages of the Avrami exponents and crystallization rate constants for the PP-rich and EPR-rich phases. In our previous work, we found that PP in the EPR-rich phase could also crystallize, leading to a coarse spherulite structure.[63] This observation shows that crystallization of PP in the EPR-rich phase is strongly confined and the growth dimension should be very small, leading to the Avrami exponents much smaller than the expected values.

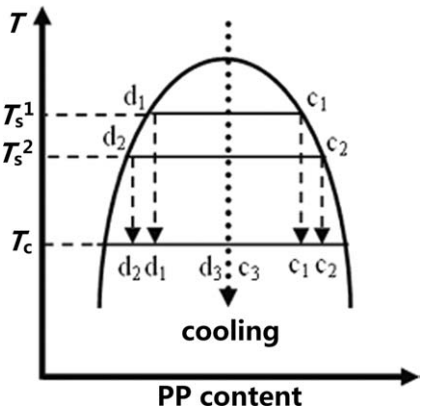

Figure 6. Schematic phase diagram for the PP/EPR in-reactor alloys.

However, at higher crystallization temperatures, secondary phase separation may take place before crystallization, because the crystallization rate is slower than the rate of phase separation. As a result, the PP contents in the PP-rich phase are the same at the same crystallization temperature, irrespectively of the phase separation temperature in the melt, and hence the previous phase separation in the melt has little effect on the linear spherulitic growth rate.[62] In this case, the nucleation rate would be the decisive factor for the differences in the overall crystallization rate under different phase separation conditions. Han and co-workers reported that phase separation may couple with crystallization and the concentration fluctuation in phase separation process would accelerate the nucleation of crystallization.[52–55] They observed in a blend system with a UCST that at a higher T_s, the rate of phase separation is lower and the degree of phase separation is smaller at the same phase separation time. When the blend is quenched from a higher T_s to T_c, the blend has a stronger tendency for further phase separation at T_c, leading to more dramatic concentration fluctuation and acceleration of nucleation for crystallization. Similarly, in the PP/EPR in-reactor alloys, the concentration fluctuation should be more dramatic when the alloys are quenched to the T_c from a higher T_s and the acceleration effect on nucleation would be more obvious. Figure 7 shows the POM images of PP/EPR in-reactor alloys of the two samples isothermally crystallized at a higher crystallization temperature ($T_c = 140$°C) for 60 min after phase separation at different temperatures for 1 h. The data for the number of spherulites in per m^3 are listed in Table II. One can see from Figure 7 and Table II that for both samples, the number of spherulites increases with the phase separation temperature in the melt. This shows that a higher T_s in the melt

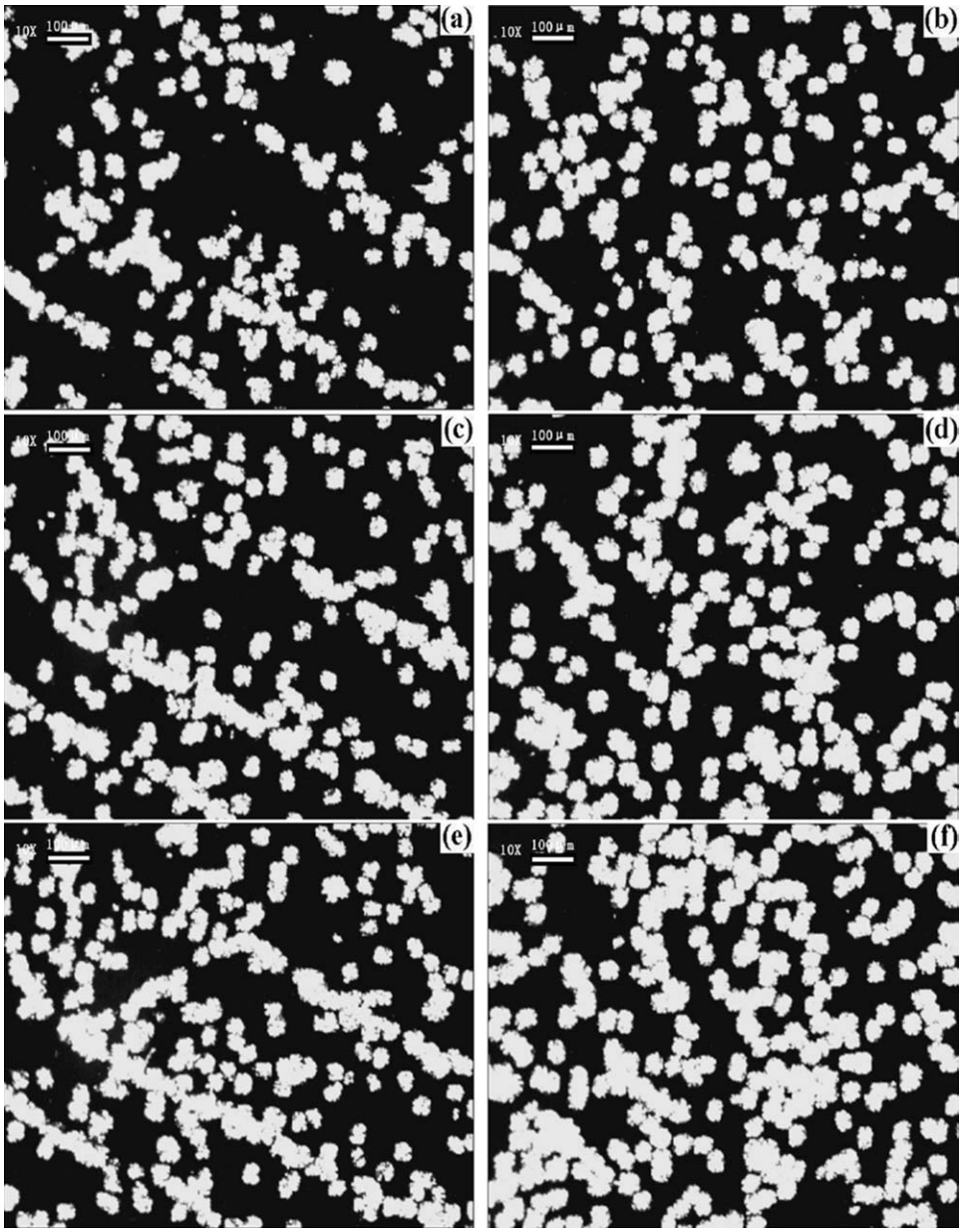

Figure 7. POM images of PP/EPR in-reactor alloys of Sample 1 [(a) $T_s = 160°C$, (c) $T_s = 170°C$, and (e) $T_s = 180°C$] and Sample 2 [(b) $T_s = 160°C$, (d) $T_s = 170°C$, (f) $T_s = 180°C$] isothermally crystallized at 140°C for 60 min after phase separation at different temperatures for 1 h.

can indeed promote nucleation of crystallization more efficiently. Therefore, we can draw the conclusion that higher nucleation rate is at least one of the dominant factors responsible for the larger overall crystallization rate at higher T_s when the PP/EPR in-reactor alloys crystallize at higher T_cs.

It is observed that in Figures 4 and 5, both Avrami exponent and crystallization rate constant increase as T_s increases at higher T_cs. This shows that both n and k contribute to the smaller $t_{1/2}$ at higher T_ss. Based on Avrami theory, the Avrami exponent is related to nucleation mechanism and growth dimension of the polymer crystals. Phase separation-assisted concentration fluctuation will enhance homogeneous nucleation, leading to a larger value of n. This is in accordance with the

Table II. The Number of Spherulites for PP/EPR In-Reactor Alloys After Isothermal Crystallization at T_c = 140°C for 1 h with Previous Phase Separation at Various Temperatures for 1 h

Sample	T_s (°C)	Thickness of sample (μm)	The number of spherulites ($10^{12}/m^3$)
Sample 1	160	30	2.90
	170	30	4.12
	180	30	5.57
Sample 2	160	31	3.75
	170	31	4.92
	180	31	6.79

Table III. Crystallization Enthalpies and Melting Points of Samples Obtained During the Isothermal Crystallization After Phase Separation at Different Temperatures for 1 h[a]

Sample	T_c (°C)	T_s (°C)	$(\Delta H_c)_{0.1}$ (J/g)	$(\Delta H_c)_{1/2}$ (J/g)	$(\Delta H_c)_{0.8}$ (J/g)	T_m (°C)
Sample 1	113	160	8.6	39.7	62.8	160.4
		170	8.0	38.9	62.3	160.6
		180	7.6	38.0	61.0	161.0
	115	160	8.0	37.5	60.3	161.1
		170	7.5	36.9	58.7	161.4
		180	7.2	36.0	57.5	161.7
	130	160	7.2	35.8	57.4	164.8
		170	8.0	39.9	63.8	165.5
		180	8.2	40.9	65.4	165.6
	133	160	8.2	39.5	63.3	167.3
		170	9.0	41.2	65.9	167.3
		180	9.5	47.4	75.8	167.5
Sample 2	113	160	9.0	41.5	67.6	160.4
		170	8.8	41.2	65.5	160.7
		180	7.8	38.9	62.0	161.1
	115	160	8.8	40.7	64.0	161.6
		170	8.2	39.9	63.9	161.5
		180	8.0	39.6	62.9	161.4
	130	160	8.1	41.6	60.8	165.4
		170	8.4	42.8	66.9	165.3
		180	8.7	43.9	69.8	165.2
	133	160	8.4	41.8	66.9	167.0
		170	9.1	45.4	72.6	166.7
		180	9.4	47.1	75.4	167.0

[a] $(\Delta H_c)_{0.1}$, $(\Delta H_c)_{1/2}$, and $(\Delta H_c)_{0.8}$ are the crystallization enthalpies at $X(t) = 0.1$, 0.5, and 0.8, where $X(t)$ is the relative crystallinity in eq. (1).

result from Figure 7. However, at higher T_cs, the increase of k with T_s seems contradict with the similar linear spherulitic growth rates at different T_ss, as reported in our previous work.[62] Again, the apparent k obtained by DSC is not only related to linear spherulitic growth rate of PP in the PP-rich phase but also dependent on the growth rate of PP crystals in the EPR-rich phase. As mentioned above, secondary phase separation may take place before crystallization at higher T_cs. Usually two-step phase separation will result in a smaller domain size, though the compositions of the phases are the same as those from the single step phase separation.[66] At lower T_s, the first phase separation at T_s will occur more completely due to deeper quenching. Therefore, it is expected that smaller domain size of the EPR-rich phase will be obtained at lower T_s, leading to a smaller value of k for the EPR-rich phase and as well as the smaller value of the apparent k. This can be seen from the effect of T_s on crystallization enthalpy (Table III). It is found that at higher T_cs (such as T_c = 130°C and T_c = 133°C), the crystallization enthalpy slightly decreases with increasing T_s, though the crystallization temperatures are the same. We believe that this originates from the retardance of crystallization in the EPR-rich phase as a result of stronger morphological confinement.

Effect of Phase Separation Time

Figure 8 presents the crystallization half-time $t_{1/2}$ of the two samples crystallized at various temperatures after phase separation at 180°C for different times. For comparison, the data of $t_{1/2}$ for the PP/EPR in-reactor alloys directly quenched from 230°C without phase separation in the melt were given as well. In Figure 8(a), it is found that $t_{1/2}$ of Sample 1 increases slightly with prolonging phase separation time, suggesting the suppression of crystallization rate. Such a phenomenon can be explained from the viewpoint of phase separation degree with time. At shorter phase separation time, the degree of phase

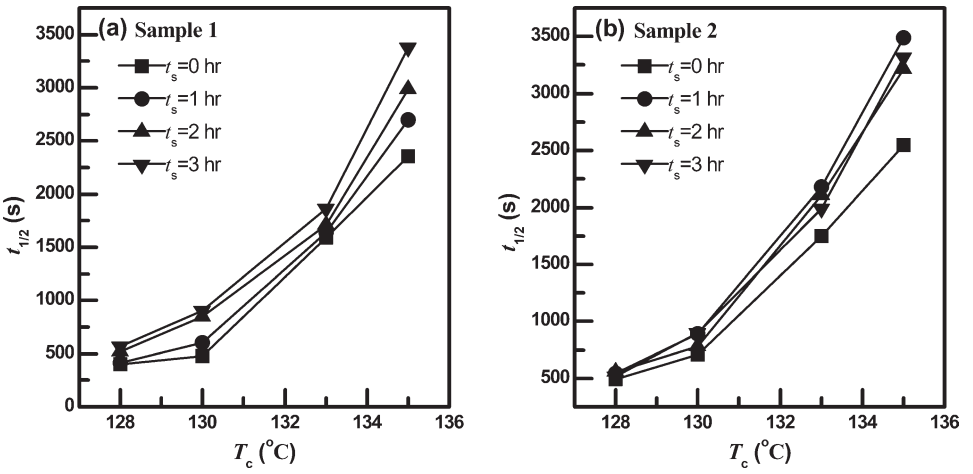

Figure 8. Effect of phase separation time on crystallization half-time of PP/EPR in-reactor alloys after phase separation at 180°C for different times. (a) Sample 1 and (b) Sample 2.

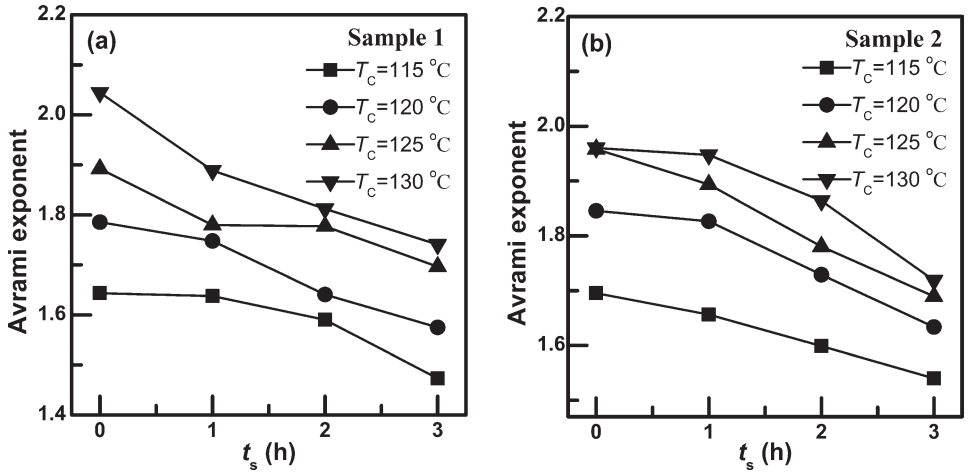

Figure 9. Plots of Avrami exponents versus phase separation time for PP/EPR in-reactor alloys after phase separation at 180°C. (a) Sample 1 and (b) Sample 2.

separation is not complete. When the PP/EPR in-reactor alloy is cooled to T_c, the secondary phase separation occurs easily, resulting in more dramatic concentration fluctuation and accordingly stronger nucleation effect. Finally, larger overall crystallization rate would be obtained at shorter phase separation time. In Figure 8(b), at the same T_c, the value of $t_{1/2}$ for the directly quenched samples is the smallest, compared with those undergoing phase separation before crystallization. This shows that the overall crystallization rate of the directly quenched samples is the largest. However, when the phase separation time extends from 1 to 3 h, there is no obvious difference among the values of $t_{1/2}$ for Sample 2, which is different from Sample 1. This may be due to the different phase transition temperatures of these two samples. Sample 2 has a higher phase transition temperature than Sample 1, thus the phase separation rate of Sample 2 is higher at $T_s = 180$°C because of its larger quench depth. Hence, phase separation may be almost completed for Sample 2 with annealing at 180°C for 1 h, resulting in no obvious change with prolonging t_s.

Figures 9 and 10 show the effects of phase separation time on the Avrami exponent and crystallization rate constant. One can see that the Avrami exponent decreases as phase separation time increases at all T_cs studied. The variation of k with T_s exhibits a similar tendency. However, the effect of phase separation time on k is much weaker than that on n, especially at lower T_cs. As a result, the slower overall crystallization rate at longer phase separation time is mainly due to the smaller n. The decrease of n with phase separation time originates from two aspects. First, the nucleation rate is retarded by longer time phase separation, as mentioned above. Second, well phase-separated morphology will have a stronger confinement effect on crystallization of the EPR-rich phase, leading to a smaller n of this phase and accordingly a smaller apparent n.

SAXS Results

The data in Figure 8 shows that the directly quenched PP/EPR alloys have a faster overall crystallization rate than the phase-separated ones at higher T_cs. To further solidify this conclusion, time-resolved SAXS experiments were conducted. Figure 11

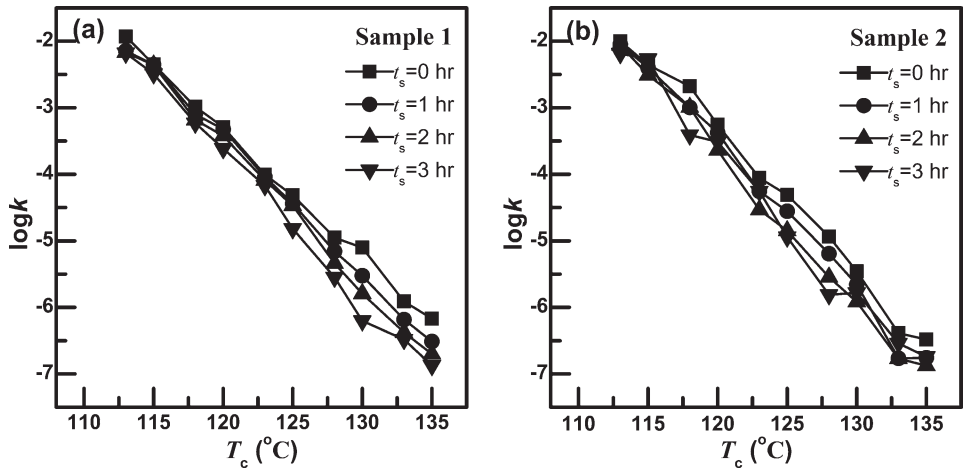

Figure 10. Plots of log k versus crystallization temperatures for PP/EPR in-reactor alloys after phase separation at 180°C for different time. (a) Sample 1 and (b) Sample 2.

Applied Polymer SCIENCE

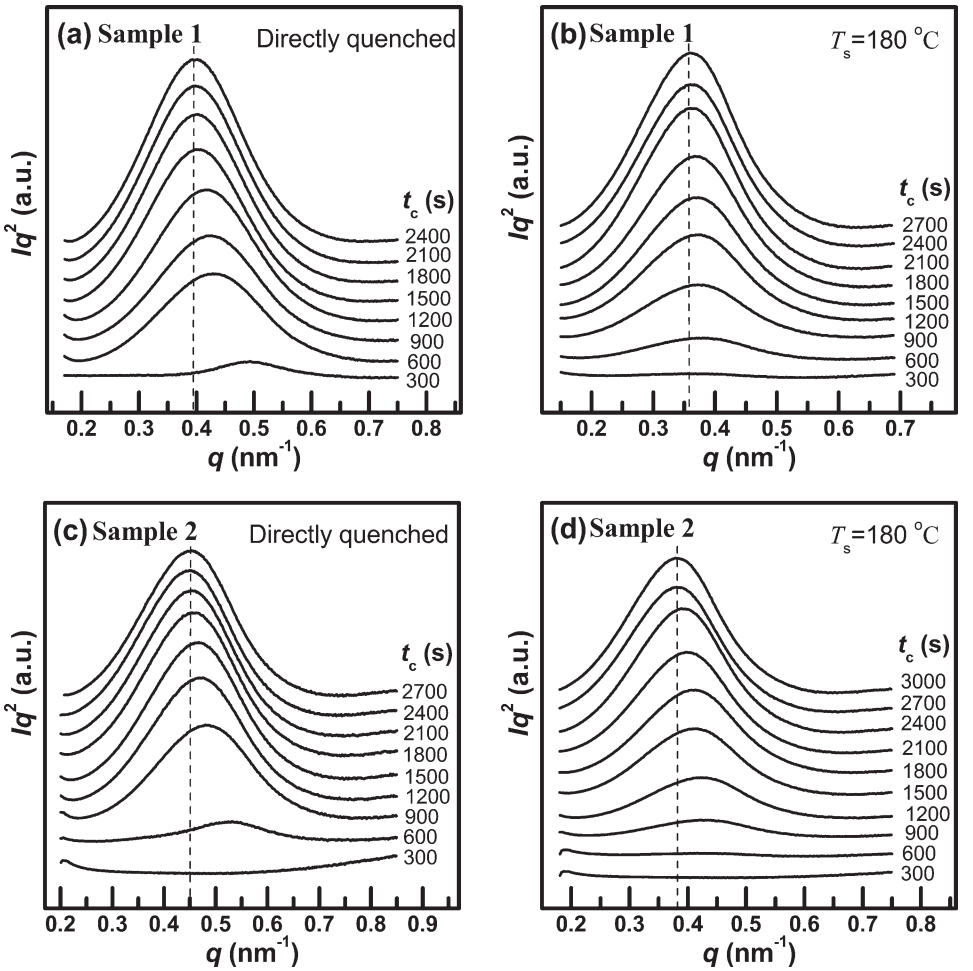

Figure 11. SAXS profiles for PP/EPR in-reactor alloys isothermal crystallization at 140°C. The figures (a) and (b) are for Sample 1 and the figures (c) and (d) are for Sample 2.

shows the Lorentz-corrected 1D SAXS profiles for samples isothermally crystallized at 140°C. Because longer exposure time is needed for each scan, the time-resolved SAXS experiment cannot be conducted at lower T_c due to the fast crystallization rate, thus only the data at a high T_c (T_c = 140°C) are presented. As shown in Figure 11, the intensity of the SAXS peak gradually becomes stronger and the position shifts to lower q with crystallization time increasing.

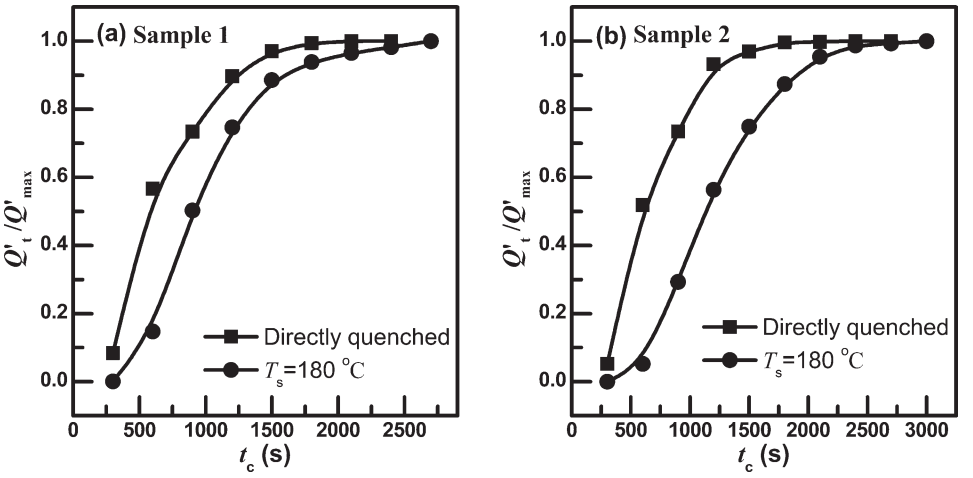

Figure 12. Plots of relative scattering invariant versus crystallization time for PP/EPR in-reactor alloys isothermally crystallized at 140°C. (a) Sample 1 and (b) Sample 2.

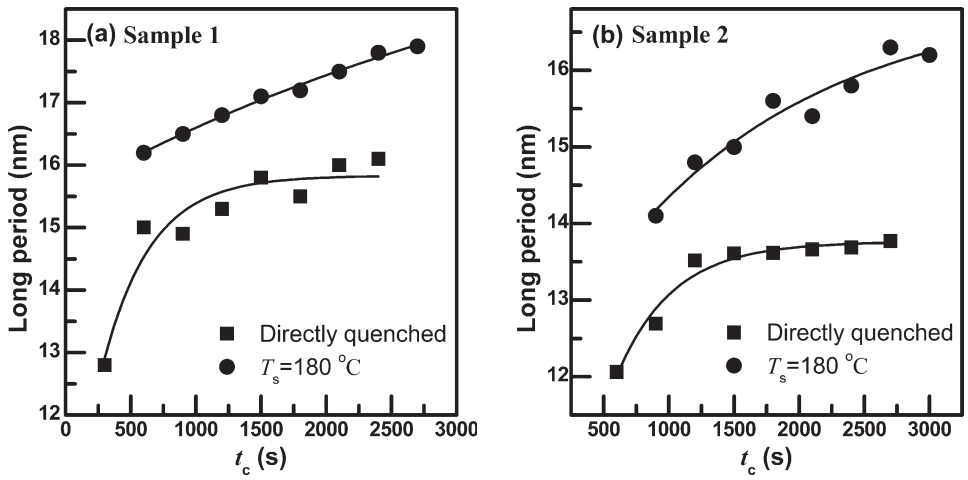

Figure 13. Plots of the long periods versus crystallization time for PP/EPR in-reactor alloys isothermally crystallized at 140°C. (a) Sample 1 and (b) Sample 2.

One can see from eq. (6) that the scattering invariant Q is proportional to the volume fraction crystallinity when ϕ_c is smaller than 0.5, which is the case of the present study. Hence, the scattering invariant Q can reflect crystallinity to some extent. We normalize the scattering invariants to yield the relative scattering invariants through dividing the scattering invariant at a certain crystallization time (Q_t') by the scattering invariant for the last exposure (Q_{max}'). Figure 12 shows the plots of the relative scattering invariant versus crystallization time for PP/EPR in-reactor alloys. It can be seen from Figure 12 that, at the same crystallization time, the relative scattering invariant of the directly quenched sample is always higher than that of the phase-separated sample. This finding holds true for both PP/EPR in-reactor alloys. This indicates that phase separation at 180°C before crystallization slows down the crystallization rate, when compared with the directly quenched sample. As a consequence, the SAXS result is in accordance with the DSC result (Figure 8).

From the SAXS peak position (q_{max}), the long period L can be calculated according to the equation $L = 2\pi/q_{max}$. Figure 13 illustrates the variations of the long period with crystallization time for both PP/EPR in-reactor alloys isothermally crystallized at 140°C. It is obvious that phase separation at 180°C for 1 h leads to larger values of long period (Figure 13), when compared with the long period of the directly quenching samples. However, we also find that phase separation in the melt before crystallization hardly affects the melting temperature of the PP crystals (Table III), as long as the crystallization temperatures are the same. Moreover, the Hoffman-Weeks plots also show that the equilibrium melting temperatures are similar for the directly quenched sample and the sample with phase separation for 1 h before crystallization. This implies that the lamellar thicknesses of the PP crystals are similar for the directly quenched and the phase-separated ones. Since the long period is the sum of the lamellar thickness of the crystals and the thickness of the amorphous layers sandwiched by the crystals, the larger long period of the phase-separated sample is due to the thicker amorphous layer. In our previous work, we found that phase separation before crystallization led to higher PP content of the EPR-rich phase and larger viscosity of this phase, thus more EPR-rich phases were included into the spherulites, resulting in a coarse spherulitic structure.[63] The SAXS result shows that more amorphous phases are included between the lamellar crystals as well. The effect of the phase separation on the long period and morphology can be schematically depicted as Figure 14.

Comparing Figure 13(a,b), one can also see that the long periods of Sample 1 is larger than those the Sample 2, irrespectively of the thermal treatment. This is due to the higher PP content in the EPR-rich phase of Sample 1 than in the Sample 2 at the same temperature, which can be seen from the phase diagram. Therefore, the EPR-rich phase can be included into the spherulites and among the lamellar crystals more easily in Sample 1 than in Sample 2, leading to a larger long period of Sample 1.

CONCLUSIONS

The DSC result shows that the effect of phase separation on the overall crystallization rate of PP/EPR in-reactor alloys strongly depends on crystallization temperature. At lower T_cs, the overall crystallization rate decreases with increasing phase separation temperature. The decrease of linear spherulitic growth rate with increasing T_s is the predominant factor responsible for this. In contrast, at higher T_c, the overall crystallization rate increases

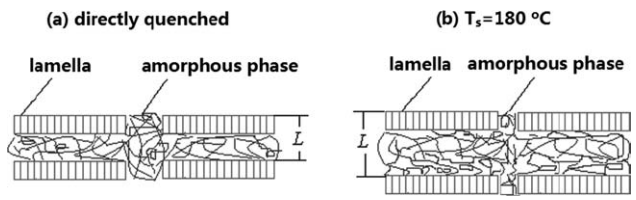

Figure 14. Schematic models for long period of PP/EPR in-reactor alloys with different thermal treatment processes. (a) PP/EPR in-reactor alloys under directly quench process and (b) PP/EPR in-reactor alloys with phase separation at 180°C for 1 h.

with increasing phase separation temperature and this can be mainly attributed to the promotion of nucleation at higher phase separation temperature. Analysis of the crystallization kinetics data shows that the EPR-rich phase also contributes to overall crystallization rate, such as considerably smaller Avrami exponent. Prolongation of phase separation time retards crystallization rate of PP/EPR in-reactor alloys. Such an effect is more obvious for the sample prepared by MSSP process, which has a lower phase transition temperature. The SAXS result verifies that the crystallization rate at higher T_c is slowed down when the PP/EPR in-reactor alloys undergo phase separation before crystallization, when compared with the directly quenched sample. More amorphous phases may also be included into the lamellar crystals due to phase separation, leading to a larger long period.

ACKNOWLEDGMENTS

Contract grant sponsor: National Natural Science Foundation of China; contract grant number: 51073138. Contract grant sponsor: National Basic Research Program of China (973 Program); contract grant number: 2011CB606005. Contract grant sponsor: Beamline BL16B1 at Shanghai Synchrotron Radiation Facility (SSRF); contract grant number: 10sr0132.

REFERENCES

1. Galli, P.; Haylock, J. C. *Prog. Polym. Sci.* **1991,** *16*, 443.
2. Galli, P.; Haylock, J. C. *Makromol. Chem. Macromol. Symp.* **1992,** *63*, 19.
3. Yokoyama, Y.; Ricco, T. *J. Appl. Polym. Sci.* **1997,** *66*, 1007.
4. Cai, H. J.; Luo, X. L.; Chen, X. X.; Ma, D. Z.; Wang, J. M.; Tan, H. S. *J. Appl. Polym. Sci.* **1999,** *71*, 103.
5. Fan, Z. Q.; Zhang, Y. Q.; Xu, J. T.; Wang, H. T.; Feng, L. X. *Polymer* **2001,** *42*, 5559.
6. Pires, M.; Mauler, R. S.; Liberman, S. A. *J. Appl. Polym. Sci.* **2004,** *92*, 2155.
7. Tan, H. S.; Li, L.; Chen, Z. N.; Song, Y. H.; Zheng, Q. *Polymer* **2005,** *46*, 3522.
8. Urdampilleta, I.; Gonzalez, A.; Iruin, J. J.; de la Cal, J. C.; Asua, J. M. *Macromolecules* **2005,** *38*, 2795.
9. Doshev, P.; Lohse, G.; Henning, S.; Krumova, M.; Heuvelsland, A.; Michler, G.; Radusch, H. J. *J. Appl. Polym. Sci.* **2006,** *101*, 2825.
10. Jiang, T.; Chen, H. X.; Ning, Y. N.; Kuang, D. T.; Qu, G. M. *J. Appl. Polym. Sci.* **2006,** *101*, 1386.
11. Cui, N. N.; Ke, Y. C.; Lu, Z. X.; Wu, C. H.; Hu, Y. L. *J. Appl. Polym. Sci.* **2006,** *100*, 4804.
12. Zhu, H. J.; Monrabal, B.; Han, C. C.; Wang, D. J. *Macromolecules* **2008,** *41*, 826.
13. Chen, Y.; Chen, Y.; Chen, W.; Yang, D. C. *J. Appl. Polym. Sci.* **2008,** *108*, 2379.
14. Song, S. J.; Feng, J. C.; Wu, P. Y.; Yang, Y. L. *Macromolecules* **2009,** *42*, 7067.
15. Song, S. J.; Wu, P. Y.; Feng, J. C.; Ye, M. X.; Yang, Y. L. *Polymer* **2009,** *50*, 286.
16. Song, S. J.; Feng, J. C.; Wu, P. Y. *Polymer* **2010,** *51*, 5267.
17. Shangguan, Y. G.; Tao, L. Y.; Zheng, Q. *J. Appl. Polym. Sci.* **2007,** *106*, 448.
18. Zhang, C. H.; Shangguan, Y. G.; Chen, R. F.; Wu, Y. Z.; Chen, F.; Zheng, Q. A.; Hu, G. H. *Polymer* **2010,** *51*, 4969.
19. Zheng, Q.; Lin, Z. H.; Peng, M. *Polym. Int.* **2004,** *53*, 1087.
20. Zheng, Q.; Shangguan, Y.; Yan, S. K.; Song, Y. H.; Peng, M.; Zhang, Q. B. *Polymer* **2005,** *46*, 3163.
21. Mirabella, F. M.; McFaddin, D. C. *Polymer* **1996,** *37*, 931.
22. Zacur, R.; Goizueta, G.; Capiati, N. *Polym. Eng. Sci.* **2000,** *40*, 1921.
23. Zhu, H. J.; Yang, H. R.; Zhao, Y.; Wang, D. J. *J. Appl. Polym. Sci.* **2011,** *121*, 1372.
24. Tian, Z.; Gu, X. P.; Wu, G. L.; Feng, L. F.; Fan, Z. Q.; Hu, G. H. *Ind. Eng. Chem. Res.* **2011,** *50*, 5992.
25. Chen, R. F.; Shangguan, Y. G.; Zhang, C. H.; Chen, F.; Harkin-Jones, E.; Zheng, Q. *Polymer* **2011,** *52*, 2956.
26. Tong, C. Y.; Lan, Y.; Chen, Y.; Yang, D. C.; Yang, X. N. *J. Appl. Polym. Sci.* **2012,** *123*, 1302.
27. Cheng, D.; Feng, J. C.; Yi, J. J. *J. Appl. Polym. Sci.* **2012,** *123*, 1784.
28. Lu, X. Y.; Yi, J. J.; Chen, S. T.; Zu, F. H.; Li, R. B. *Chin. J. Polym. Sci.* **2012,** *30*, 122.
29. Simonazzi, T.; Cecchin, G.; Mazzullo, S. *Prog. Polym. Sci.* **1991,** *16*, 303.
30. Galli, P.; Vecellio, G. *Prog. Polym. Sci.* **2001,** *26*, 1287.
31. Fu, Z. S.; Fan, Z. Q.; Zhang, Y. Q.; Feng, L. X. *Eur. Polym. J.* **2003,** *39*, 795.
32. Fu, Z. S.; Fan, Z. Q.; Zhang, Y. Z.; Xu, J. T. *Polym. Int.* **2004,** *53*, 1169.
33. Galli, P. *J. Macromol. Sci. Pure Appl. Chem.* **1999,** *A36*, 1561.
34. Covezzi, M.; Mei, G. *Chem. Eng. Sci.* **2001,** *56*, 4059.
35. Fernandes, F. A. N.; Lona, L. M. F. *J. Appl. Polym. Sci.* **2004,** *93*, 1042.
36. Fernandes, F. A. N.; Lona, L. M. F. *J. Appl. Polym. Sci.* **2004,** *93*, 1053.
37. Santos, J. L.; Asua, J. M.; de la Cal, J. C. *Ind. Eng. Chem. Res.* **2006,** *45*, 3081.
38. Dong, Q.; Wang, X. F.; Fu, Z. S.; Xu, J. T.; Fan, Z. Q. *Polymer* **2007,** *48*, 5905.
39. Xu, J. T.; Feng, L. X.; Yang, S. L.; Wu, Y. N.; Yang, Y. Q.; Kong, X. M. *Polymer* **1997,** *38*, 4381.
40. Mirabella, F. M. J. *Polymer* **1993,** *34*, 1729.
41. Xu, J. T.; Feng, L. X. *Polym. Int.* **1998,** *47*, 433.
42. Cai, H. J.; Luo, X. L.; Ma, D. Z.; Wang, J. M.; Tan, H. S. *J. Appl. Polym. Sci.* **1999,** *71*, 93.
43. de Goede, E.; Mallon, P.; Pasch, H. *Macromol. Mater. Eng.* **2010,** *295*, 366.
44. Garcia, R. A.; Coto, B.; Exposito, M. T.; Suarez, I.; Fernandez-Fernandez, A.; Caveda, S. *Macromol. Res.* **2011,** *19*, 778.

45. Tanaka, H.; Nishi, T. *Phys. Rev. Lett.* **1985,** *55*, 1102.
46. Tanaka, H.; Nishi, T. *Phys. Rev. A* **1989,** *39*, 783.
47. Inaba, N.; Sato, K.; Suzuki, S.; Hashimoto, T. *Macromolecules* **1986,** *19*, 1690.
48. Inaba, N.; Yamada, T.; Suzuki, S.; Hashimoto, T. *Macromolecules* **1988,** *21*, 407.
49. Crist, B.; Hill, M. J. *J. Polym. Sci. Part B: Polym. Phys.* **1997,** *35*, 2329.
50. Shimizu, K.; Wang, H.; Wang, Z. G.; Matsuba, G.; Kim, H.; Han, C. C. *Polymer* **2004,** *45*, 7061.
51. Wang, Z. G.; Wang, H.; Shimizu, K.; Dong, J. Y.; Hsiao, B. S.; Han, C. C. *Polymer* **2005,** *46*, 2675.
52. Zhang, X. H.; Wang, Z. G.; Muthukumar, M.; Han, C. C. *Macromol. Rapid Commun.* **2005,** *26*, 1285.
53. Zhang, X. H.; Wang, Z. G.; Dong, X.; Wang, D. J.; Han, C. C. *J. Chem. Phys.* **2006,** *125*, 024907.
54. Niu, Y. H.; Wang, Z. G.; Orta, C. A.; Xu, D. H.; Wang, H.; Shimizu, K.; Hsiao, B. S.; Han, C. C. *Polymer* **2007,** *48*, 6668.
55. Shimizu, K.; Wang, H.; Matsuba, G.; Wang, Z. G.; Kim, H.; Peng, W. Q.; Han, C. C. *Polymer* **2007,** *48*, 4226.
56. Du, J.; Niu, H.; Dong, J. Y.; Dong, X.; Wang, D.; He, A.; Han, C. C. *Macromolecules* **2008,** *41*, 1421.
57. Du, J.; Zhang, X. H.; Han, C. C. *J. Polym. Sci. Part B: Polym. Phys.* **2009,** *47*, 166.
58. Luo, J.; Liang, Y. R.; Yang, J. J.; Niu, H.; Dong, J. Y.; Han, C. C. *Polymer* **2011,** *52*, 4590.
59. Xu, J. T.; Fu, Z. S.; Wang, X. P.; Geng, J. S.; Fan, Z. Q. *J. Appl. Polym. Sci.* **2005,** *98*, 632.
60. Lin, Z. H.; Peng, M.; Zheng, Q. *J. Appl. Polym. Sci.* **2004,** *93*, 877.
61. Shangguan, Y. G.; Song, Y. H.; Zheng, Q. *Polymer* **2007,** *48*, 4567.
62. Liu, Y. M.; Li, Y.; Xu, J. T.; Fu, Z. S.; Fan, Z. Q. *J. Appl. Polym. Sci.* **2012,** *123*, 535.
63. Li, Y.; Xu, J. T.; Dong, Q.; Fu, Z. S.; Fan, Z. Q. *Polymer* **2009,** *50*, 5134.
64. Avrami, M. *J. Chem. Phys.* **1939,** *7*, 1103.
65. Ryan, A. J.; Stanford, J. L.; Bras, W.; Nye, T. M. W. *Polymer* **1997,** *38*, 759.
66. Cheng, S. Z. D. Phase Transitions in Polymers: The Role of Metastable States; New York: Elsevier, **2008.**